

# Development of a mathematical model of flow, heat transfer and combustion in a stratified charge engine

Benjamin, S.F. , Weaving, J.H. , Glynn, D.R. , Markatos, N.C. and Spalding, D.B.

**Published version deposited in CURVE June 2013**

## **Original citation & hyperlink:**

Benjamin, S.F. Weaving, J.H. Glynn, D.R. Markatos, N.C. Spalding, D.B. (1980) Development of a mathematical model of flow, heat transfer and combustion in a stratified charge engine. Proc. Inst. Mech. Engineers. Conf. on Stratified Charge Automotive Engines; 11/1980.  
<http://www.imeche.org/>

## **Additional note**

Please note Professor Benjamin was working at BL Technology Limited at the time of publication.

**Copyright © and Moral Rights are retained by the author(s) and/ or other copyright owners. A copy can be downloaded for personal non-commercial research or study, without prior permission or charge. This item cannot be reproduced or quoted extensively from without first obtaining permission in writing from the copyright holder(s). The content must not be changed in any way or sold commercially in any format or medium without the formal permission of the copyright holders.**

**CURVE is the Institutional Repository for Coventry University**

<http://curve.coventry.ac.uk/open>

# DEVELOPMENT OF A MATHEMATICAL MODEL OF FLOW, HEAT TRANSFER AND COMBUSTION IN A STRATIFIED CHARGE ENGINE

S. F. BENJAMIN and J. H. WEAVING

BL Technology Limited

D. R. GLYNN, N. C. MARKATOS and D. B. SPALDING

Concentration, Heat and Momentum Limited

## SYNOPSIS

This paper presents a method for calculating the transient, turbulent flow, heat transfer and combustion processes in the main and pre-chambers of a stratified charge engine. The calculation takes place in a two-dimensional plane normal to the main chamber axis, with motion of the piston being taken into account. The method includes models for calculating the movement of the flame front as it passes through the mixture, and also for the controlling processes of chemical kinetics, turbulence, and wall heat and momentum transfer. The predictions are compared with experimental data under engine motoring conditions. Firing conditions have been attempted and some values of gas velocity obtained. It is demonstrated that this method has the potential for predicting flame velocities under turbulent conditions.

## INTRODUCTION

### 1.1 Background

The field of numerical modelling of combustion in internal combustion engines is now developing rapidly (1,2). The interest has been motivated by the recognition that numerical models may be essential for the development of cleaner, less noisy and more efficient engines for a variety of designs and fuels. A great advantage of such an approach is that the generality required by the many applications is matched by the generality of models. They can be applied to reciprocating or rotary engines, with uniform or stratified charges, with open or divided chambers.

The flow and combustion processes in a double chamber stratified charge engine are of interest at present, since this type of engine offers a method for reducing fuel consumption and pollutant emissions by enabling ignition to take place in a region with a higher fuel concentration than in the main burning region.

Combustion is very different in this engine than in a normal homogeneous charge engine. Although a major part of the combustion takes place in the main chamber, the mode of ignition by a spark, and the precise mode of the spread of the flame is not yet adequately understood. A mathematical model would aid the designer of a stratified charge engine; it would, for instance, enable him to study the effects of varying the geometry of the chambers without the need to set up a large number of experiments, to investigate such important practical matters as the effects of turbu-

lence and charge stratification, and to predict flame propagation.

Against this background, British Leyland Advanced Technology Laboratory have become aware of the necessity for a full investigation of the processes occurring in a stratified charge engine and invited Concentration, Heat and Momentum Limited to develop such a mathematical model. In order to assess quantitatively the accuracy of the developed model, BL Technology have performed experimental measurements of the flow fields in the engine, and the outcome of this collaboration is presented in this paper.

### 1.2 Objectives of the Work and Purpose of the Paper

The purpose of the work is the development and validation of a mathematical model for the prediction of the combustion processes in a pre-chamber type of stratified charge engine.

The broad objectives of BL's stratified charge engine programme is to obtain reduced emissions with increased fuel economy. The stratified charge engine is regarded as one promising way of approaching diesel engine efficiency without the expense of a heavier engine and expensive injection equipment, and at the same time achieving lower carbon monoxide and nitric oxide emissions. This is possible by controlling the engine over its load range by reducing the fuel supply to the carburettor while maintaining the throttle as nearly as possible fully open. This increases the thermodynamic efficiency due to the higher ratio of the specific heats and reduced pumping losses (3). However, the very lean burning at low loads means that in practice some throttling becomes necessary. Weak mixtures normally slow down combustion with consequent loss of efficiency. It is hoped that the model will point the way of restoring burning speeds and thus bringing the process nearer to the constant velocity cycle, thereby achieving greater efficiency than is possible in a conventional engine which does not normally burn weaker than about 18/1 air-fuel ratio (AFR).

The purpose of the present paper is to describe the mathematical and numerical aspects of the model, and to illustrate its capabilities, limitations and potential by comparing predictions with experiments for both a motored-model-engine and for a model under firing conditions.

### 1.3 Contents of Paper

The remainder of this paper consists of three sections. Section 2 is devoted to the description of the method, starting from the choice of model, proceeding through the description of the governing differential equations and the numerical solution technique and ending with the modelling of the combustion process. Validation of the model is then presented in Section 3, including: validation with the engine motoring and under firing conditions.

The concluding Section 4 summarises the current status of the method and suggests directions of future developments.

## 2. DESCRIPTION OF METHOD

### 2.1 Choice of Model - The Present Approach

Figure 1 shows the type of stratified charge engine under investigation in the BL Advanced Technology Laboratory which has been the subject of a previous paper (3). In this type of engine, with a pre-chamber that discharges into the main chamber, it is clear that there will be considerable movement of the gas, and that a two-zone model dividing the volume of the combustion chamber into burnt and unburnt charges would not adequately represent the physical phenomena actually taking place. Instead, a method which solves the full partial differential equations governing the flow is required.

The flow is three-dimensional and time-dependent. Although the system may be modelled three-dimensionally, a two-dimensional model of the flow has been considered at this stage, in a plane normal to the main chamber axis.

As the main chamber is confined between two parallel planes, namely, the flat head and the piston, the two-dimensional approach is considered adequate for the present, given that it allows thermodynamically for the increase in volume due to the piston motion in the third direction. The approach becomes more justifiable also because the major interest is in the combustion period between  $30^\circ$  before TDC and  $30^\circ$  after, when the piston is near to the cylinder head. The advantage of this approach is that it can, within the limitations of the assumptions involved, depict the actual phenomena of both gas dynamics and combustion in space and time; while being more economical in computer time and storage, and simpler to use, than its three-dimensional counterpart.

### 2.2 Mathematical Representation of Stratified Charge Processes

#### 2.2.1 The dependent variables

The following are the dependent variables, for which conservation equations are solved:

- the axial and lateral velocity components,  $u$  and  $v$ ;
- the pressure,  $p$ ;
- the stagnation enthalpy,  $\tilde{h}$ ;
- the turbulence energy,  $k$ , and its dissipation rate,  $\epsilon$ ;

- the mixture fraction,  $f$ ; and,
- the concentration of reactant fuel and other gaseous species,  $m_{fu}$ ,  $m_N$ ,  $m_{NO}$ .

#### 2.2.2 Governing equations

The continuity equation is:

$$\frac{D\rho}{Dt} + \rho \operatorname{div} \underline{u} = 0. \quad (1)$$

$$\underline{u} \equiv (u, v); \operatorname{div} \underline{u} \equiv \frac{\partial u}{\partial x} + \frac{\partial v}{\partial y}$$

The other conservation equations may all be expressed in the form:

$$\frac{\partial (\rho \phi)}{\partial t} + \operatorname{div} (\rho \underline{u} \phi - \underline{J} \phi) = S_\phi \quad (2)$$

$$\underline{J} \phi \equiv \left( \frac{\partial \phi}{\partial x}, \frac{\partial \phi}{\partial y} \right)$$

Here,  $\phi$  is the exchange coefficient,  $S_\phi$  is the source term of the dependent variable  $\phi$ . Expressions for  $\underline{J}$  and  $S_\phi$  are shown in Table 1. Here  $\sigma$  is the laminar Prandtl number and the symbols  $\mu$ ,  $\mu_t$  and  $\mu_{eff}$  stand respectively for the laminar, turbulent and effective values of viscosity.  $G_k$  is the generation rate of turbulence kinetic energy. The turbulent viscosity is evaluated from the local computed values of  $k$  and  $\epsilon$ , as described in the next section. The quantities  $\sigma_{t, \phi}$  are turbulent Prandtl numbers, the values which must be determined empirically as input to the turbulence-model constants are given in Table 2; these values are based on experience of calculating a wide range of turbulent flows. A detailed description of the turbulence model is given by Launder and Spalding (5).

#### 2.2.3 Auxiliary relations

The following formulae and values close the equation set:

- The effective viscosity is the sum of the laminar viscosity,  $\mu$ , and a turbulent viscosity,  $\mu_t$ , evaluated from  $k$  and  $\epsilon$ :

$$\mu_{eff} = \mu + \mu_t = \mu + C_D \frac{k^2}{\epsilon}, \quad (3)$$

where  $C_D$  is a constant, which takes the value given in Table 2.

- The generation term  $G_k$  is evaluated from:

$$G_k = 2 \left\{ \left( \frac{\partial u}{\partial x} \right)^2 + \left( \frac{\partial u}{\partial y} \right)^2 \right\} + \left( \frac{\partial u}{\partial y} + \frac{\partial v}{\partial x} \right)^2 \quad (4)$$

- The density is calculated from the equation of state:

$$\rho = p / nRT \quad (5)$$

$$\text{where } n = \frac{m_{fu}}{w_{fu}} + \frac{m_{ox}}{w_{ox}} + \dots$$

and  $w$  is the molecular weight.

- The temperature is obtained from the enthalpy as follows: (6)

$$T = (\tilde{h} - h_{fu} m_{fu} - h_{H_2} m_{H_2} - h_{CO} m_{CO} - \frac{1}{2}(u^2 + v^2)) / c_p$$

where  $c_p$  is the specific heat, and  $h_{fu}$  is the heat of combustion of the fuel.  $c_p$  is calculated as in Section 2.8 below.

#### 2.2.4 Boundary conditions

The mathematical modelling of a particular engine also requires a statement of the conditions at its boundaries. There are two types of boundaries: (a) wall boundaries, and (b) the axis of symmetry.

The symmetry axis has a simple zero-flux condition on all variables.

At a wall, the component of velocity normal to the wall is zero, and the fluxes of chemical species, mixture fraction, turbulence fluctuations and their dissipation rate are also zero.

Wall friction and heat transfer are treated by specifying the values of the shear stress coefficient and the Stanton number. This approximation is consistent with the approximation implied by the two-dimensional assumption.

Wall functions (6) are provided for  $k$  and  $\epsilon$ .

#### 2.3 The Finite-Difference Grid

The geometry which has been considered is shown in Figure 1, which also indicates the type of grid used. The grid is non-orthogonal. The velocity components and the other variables are stored in 'staggered' positions on the grid. These storage locations, and the corresponding control volumes, are shown in Figure 2.

#### 2.4 Piston Movement

Piston movement is accounted for in two respects. First, the volumes and face-areas of the control cells in the main chamber are varied appropriately with time. Secondly, the change in volume of the control cells introduces an additional term into the continuity equation. This is discussed below in the section describing the pressure-correction equation. Finally, the changes in pressure caused by the movement of the piston are taken account of in the pressure-work term of the enthalpy equation.

#### 2.5 The Finite-Difference Equations and Their Solution.

The differential equation (2) may be integrated over a control volume, giving:

$$\int_V \text{div} (\rho \mathbf{u} \phi - \Gamma_\phi \nabla \phi) dV = \int_V (S_\phi - \frac{\partial (\rho \phi)}{\partial t}) dV. \quad (7)$$

Using the divergence theorem we obtain.

$$\sum_i (\rho \mathbf{u} \phi - \Gamma_\phi \nabla \phi)_i \cdot (\mathbf{A}_i \mathbf{n}_i) = (S_\phi - \frac{\partial (\rho \phi)}{\partial t}) \Delta V. \quad (8)$$

where the sum is over the cell faces.  $A_i$  and  $\mathbf{n}_i$  are respectively the cell face area and the unit normal to the cell face. Equation (8) can be approximated to give:

$$\phi_p = \frac{a \phi_N + b \phi_S + c + S_U}{d - S_p} \quad (9)$$

where  $\phi_p, \phi_N$  and  $\phi_S$  refer to the values of  $\phi$  at the centre of the cell and on its 'north' and 'south' faces, as shown in Figure 2. The quantities of  $a, b, c, d$  are related to the convective and diffusive fluxes of  $\phi$  through the cell faces. The values of  $\phi$  on the 'east' and 'west' faces of the cell, which occur in equation (8), are included into the co-efficient  $c$ . The quantities  $S_u$  and  $S_p$  are related to the source and transient expressions.

The equation (9) for a line of cells at constant  $x$  form a closed set of simultaneous equations which are solved to obtain the values of  $\phi$  for these cells by the tri-diagonal matrix algorithm.

#### 2.6 Pressure-Correction Equation

After the velocity components have been calculated for a line of cells, the pressures are adjusted so that the continuity equation is satisfied. Suppose that  $R^*$  is the volumetric continuity error in a cell, so that

$$R^* = C_n - C_s + C_e - C_w - \frac{V}{\gamma \Delta t} \log \left( \frac{p}{p_{old}} \right) - \frac{V}{L} u_{pis}, \quad (10)$$

where  $C$  is the volume flux through cell face (see Figure 2),  $V$  is the volume of the cell,  $\Delta t$  is the time step,  $p_{old}$  is the pressure in the cell at the previous time step,  $L$  is the distance between the piston and the top of the cylinder, and  $u_{pis}$  is the piston velocity. The second term on the right-hand side of this equation represents the volume flux out of the cell due to the effects of compressibility; the derivation of this term is given by Awn (7). The third term is the change in volume of the cell due to piston movement.

It may be shown (Patankar and Spalding (6), and Spalding (8)) that:

$$R^* = c_1 \Delta p_p + c_2 \Delta p_N + c_3 \Delta p_S \quad (11)$$

where  $\Delta p_p, \Delta p_N, \Delta p_S$  are the changes in pressure at the cell under consideration and at its north and south neighbours which are necessary for the continuity error to vanish, and  $c_1, c_2, c_3$  are coefficients which may be evaluated. Then:

$$c_1 \Delta p_p + c_2 \Delta p_N + c_3 \Delta p_S = C_n - C_s + C_e - C_w - \frac{V}{\gamma \Delta t} \log \left( \frac{p}{p_{old}} \right) - \frac{V}{L} u_{pis}. \quad (12)$$

This is the pressure-correction equation. The set of equations (11) for a line of cells at constant  $x$  may be solved simultaneously for the pressure corrections  $\Delta p$ . The same tri-diagonal matrix algorithm is used.

#### 2.7 Solution Procedure

The calculation proceeds by determining the solution at successive time steps, the magnitude of the time step having been specified.

At each time step the procedure is as follows. On each line of cells at constant  $x$ , in turn, the velocities and the other variables listed in Table 1 are found by solving the finite-difference equations (9), and the pressure-correction equation (12) is then used to find the values of pressure on the line which are consistent with the continuity equation. This "sweep" of the domain gives an approximation to the solution of the equations. This approximation is then improved by making repeated sweeps of the domain until the required degree of accuracy is obtained. The calculation can then proceed with the next time step.

## 2.8 Modelling of the Combustion Process

The combustion chamber initially contains a lean mixture in the main chamber and a richer mixture in the pre-chamber. Following ignition the pre-chamber gas expands into the main chamber preceded by a flame front. Behind the flame front a slower reaction takes place in which unburnt fuel emerges from the pre-chamber and burns in any excess oxygen remaining in the main chamber. The methods of modelling these two combustion processes are now discussed.

### Flame front treatment

This is of vital importance to achieving the objectives. The flame front should reach the remote portions of the combustion chamber as quickly as possible but without causing engine roughness or detonation.

It would theoretically be possible to treat the entire combustion process, including the flame front, by solution of the equations set out in Section 2.2. The flame front is thin, and rapid changes in fluid properties occur across it. To prevent the flame front from becoming excessively smeared out due to numerical diffusion it would be necessary to use an extremely fine grid. A better approach is to track the progress of the flame explicitly, and to ensure the correct variation in properties across it.

The position of the flame front is therefore stored as a set of co-ordinates of points  $p_n$ . At each time step, each of these points is moved with the local flame velocity, which is the vector sum of the burning velocity and the local unburnt gas speed. This flame tracking is a Lagrangian approach, which contrasts with the Eulerian solution of the finite-difference equations.

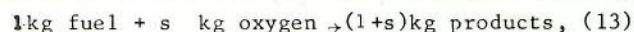
There are two components of velocity for each point on the flame front: (i) the burning speed, normal to the flame (which may be constant or a function of local turbulence, pressure, etc); and (ii) the local gas velocity, on the unburnt side of the flame. The local gas velocity is found by interpolation; the  $(x,y)$  co-ordinates of the point are then incremented appropriately.

Note that the local expansion caused by the flame makes the local gas velocities on the two sides of the flame different; it is that on the unburnt side which convects the flame and hence should be used.

When a cell is intersected by the flame front, an additional volume-source term must appear in the pressure-correction equation.

## Combustion at the flame front

At each time step, the mass-fraction of fuel burnt by the flame in each cell must be calculated, and the other dependent variables adjusted accordingly. For the mixing-controlled combustion behind the flame front a simple one-step reaction is assumed:



where  $s$  represents the stoichiometric ratio. No intermediate species are considered in this process, and the products of the reaction are considered as a single entity.

### Prediction of flame speed

A theory is required which will predict the speed of propagation of the flame under the turbulent conditions which exist in the combustion chamber. Such a theory is provided by the work of Bradley et al (9), together with that of others reviewed by him. Bradley's theory employs two sizes of eddy; one is associated with the integral scale of turbulence, the other with the Kolmogorov scale. The theory relates the turbulent and laminar flame speeds as follows:

$$\frac{u_t}{u_l} \sim \frac{u'}{u_l} \left( \frac{\epsilon}{\nu \tau_f} \right)^{0.5}$$

where  $u_t$  = turbulent flame velocity;  
 $u_l$  = laminar flame velocity;  
 $u'$  = RMS turbulent velocity;  
 $\nu$  = kinematic viscosity;  
 $\epsilon$  = turbulent diffusivity; and  
 $\tau_f$  = dimensionless time to obtain full reactivity.

The above combustion kinetics has been verified experimentally for methane in a bomb, using four high speed paddles to generate isotropic turbulence.

### Combustion behind the flame front

Behind the flame front there may be a region of distributed combustion, where incompletely burnt fuel emerging from the pre-chamber burns in the oxygen remaining in the main chamber. This process is also modelled by the simple one-step reaction (equation (13)); the transport equation (2) for mixture fraction and fuel mass-fraction are solved to predict the concentrations of the various species, and the heat release.

The solution scheme proceeds in the following manner. First, the finite-difference equations are solved for the velocity components, the turbulence quantities, and the stagnation enthalpy. Then the equations for the mixture fraction,  $f$ , and the unburnt-fuel mass fraction are solved throughout the chamber. The mixture fraction is linearly related to the difference between the local fuel concentration and the stoichiometric value, and indicates the mixing process between the two chambers. For example, since nitrogen is inert, the local mass-fraction of nitrogen is obtained from:

$$m_{N_2} = f(m_{N_2,pre} - m_{N_2,main}) + m_{N_2,main} \quad (15)$$

From the new values of  $f$  and  $m_{fu}$  the mass fraction of oxygen,  $m_{ox}$ , is found by the equation:

$$m_{ox} = s \left( m_{fu} - \frac{f-f_{st}}{1-f_{st}} \right), \quad (16)$$

where  $f_{st}$  is the stoichiometric value of  $f$ . The mixture specific heat  $C_p$  is now determined from the equation:

$$C_p = m_{fu} C_{fu} + m_{ox} C_{ox} + (1 - m_{fu} - m_{ox} - m_{N_2}) C_{pr}, \quad (17)$$

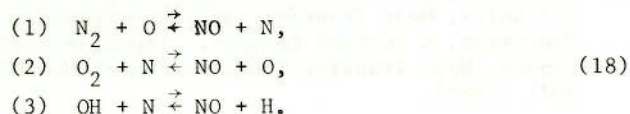
where  $C_{fu}$ ,  $C_{ox}$  and  $C_{pr}$  are the specific heats of fuel, oxygen and products respectively. Equation (17) is used together with equation (6) to determine the local temperature of the gas mixture.

The reaction rate is obtained from an Arrhenius expression.

#### Nitric oxide prediction

A chemical equilibrium analysis is performed of the products of the above reaction to estimate the concentrations of the individual species  $H$ ,  $O$ ,  $OH$ ,  $H_2$ ,  $H_2O$ ,  $CO$  and  $CO_2$ . This analysis is based on the minimisation of Gibbs free energy, and details are given in (10).

The formation of nitric oxide is then determined by use of the Zeldovich mechanism:



This is done by solving equations of the form (2) for the concentrations of  $N$  and  $NO$ , using specified reaction rates. A basic assumption made is that these reactions can be considered as decoupled from the main fuel-burning reaction, in the sense that at each time-step (while the calculation of the latter reaction will determine the  $NO_x$  produced in that time step) the  $NO_x$  calculation has no influence on the fuel-burning reaction. Other reactions, involving  $N_2O$  and  $NO_2$ , might also be considered.

### 3. VALIDATION OF THE MODEL

#### 3.1 General

The approach is to divide the process into two parts. The first is to establish the gas dynamics in the combustion chamber without combustion; this represents the situation of a motored engine. Having established the pressure and velocity fields, the process is then modified by the addition of combustion. This approach has the advantage of allowing validation of the simpler motoring conditions before adding the complication of combustion, and allows more than one combustion theory to be explored. To accomplish this a rig has been built to simulate as closely as possible the two dimensional situation. This consists of a single cylinder 'engine' with a special cylinder head that has been simplified to two cylindrical chambers joined by a parallel circular passage.

The bigger cylinder has the same diameter as the bore, but the smaller coplanar cylinder has the same volume as the pre-chamber of the actual engine. It will be appreciated that this motoring engine has been designed to fit the model in order to make comparison as valid as possible.

#### 3.2 Results and Discussion

The results obtained represent in terms of pressure, velocity and turbulence, the conditions in a running engine up to the point of spark ignition; thereafter it will represent an unreal gas motion that nevertheless should be predicted by the model. It will thus give a jet velocity from the smaller to the larger chamber as the piston descends but the velocity will be lower than that obtained in the firing engine.

Hot wire anemometry and laser doppler anemometry measurements have been taken in several places in the cylinder head of this rig and the methods and details are described in the companion paper at this conference (4).

For the simulation the flow domain was divided into a grid of  $51 \times 12$  cells. One time step was taken every half degree of crank angle. The simulation began at TDC assuming the fluid at rest. Though this is an approximation it is reasonable for the motored situation as without combustion there should be little pressure difference between the chambers at TDC. The model predicted that as the prechamber fluid emerged into the main chamber a symmetrical pair of recirculating eddies formed either side of the throat in the main chamber. The progression of the emerging jet across the main chamber and its associated velocity field are shown in figures 4 to 6. The position of the measuring points A-H are shown in figure 3. All measurements shown were obtained from the laser doppler anemometer system (LDA). Confirmatory hot wire anemometry tests were also made and are reported in ref (4).

Figure 4 shows a comparison between observations and predictions of the axial component of velocity ( $u$ ) along the axis of the main chamber. Figure 5 shows a comparison across the chamber. The predicted negative values of  $u$  at the point furthest from the axis indicates the presence of recirculation. Figure 6 shows comparisons of the lateral component of velocity (positive away from the axis of symmetry) both on and off the axis of symmetry.

The following points should be borne in mind when assessing model performance.

- Differences of the order of 30% are observed between measurements made at the same point in the chamber in different runs (see for example Figure 4, point C for which 3 runs were made).
- Significant differences were also observed between the laser doppler and the hot wire anemometry (HWA) measurements (4). For example a phase difference of 25 degrees between the peak velocity at position A between the two methods was observed. Using the HWA measurements Figure 4 shows that better correlation with regard to the timing of the peak

- c. The LDA measurements of the lateral velocity component V at position E as shown in Figure 6 indicates that the flow may be asymmetrical. The model assumes the flow field is symmetrical.

Clearly there is scope for model improvement allied with more measurements. If a recirculation region exists it is evidently more confined than the model predicts. It should also be established whether the flow field is truly symmetrical.

Validation for the combustion part of the cycle is more difficult. The model predicts spatially and temporally and validation should also do so. Therefore rather than measuring overall and average values we require to measure particular values in discrete places. Hot wire anemometry is not applicable and laser doppler methods have been used. Unfortunately at this time the few anemometry readings obtained were insufficient for validation.

Pressure is easy to measure and a comparison of observation and prediction is shown in Figure 7 for the pressure in the main chamber. Although it is ultimately intended, as indicated above to predict the appropriate flame speed in each cell as computed from turbulence and local gas conditions for a first approximation for this simulation an average constant flame velocity of 20 metres per second has been assumed. It will be seen that correlation is not bad, the small oscillations being due to movement between the main chamber and the prechamber.

The lack of precise correlation between model and measurement should not be taken as a reflection of the inadequacy of the model compared with simpler models which by adjustment of constants may be made to validate well. However neither should it be taken that the model is yet proved for accuracy. Much more has to be done, more velocity measurements, temperature measurements and experimental flame positioning are contemplated.

#### 4. CONCLUSIONS

It is realised there is a long way to go before the model will have its maximum value. However it is hoped that the importance of a grid model has been demonstrated. The model has potential for predicting flame velocities in light of the turbulent conditions and hopefully will enable the designers to design combustion chambers to give an appropriate amount of turbulence to achieve maximum efficiency on the best basis of compromise for pollutant emissions.

#### 5. ACKNOWLEDGEMENTS

The authors wish to acknowledge the contribution made by W J Corkill and K J Bullock of BL Technology Limited and Dr G Wigley of AERE Harwell for the painstaking experimental work with HWA and LDA that has been used in this paper.

Finally they would like to thank the Directors of British Leyland for permission to publish this paper.

1. Gosman A D, Johns R J R, Tipler W and Watkins A P "Computer Simulation of In-Cylinder Flow, Heat Transfer and Combustion: A Progress Report". 13th International Congress on Combustion Engines, CIMAC, Vienna 1979.
2. Syed S A and Bracco F V "Further Comparisons of Computed and Measured Divided-Chamber Engine Combustion". SAE Technical Paper Series, No 790247, 1979.
3. Weaving J H and Corkill W J "British Leyland Experimental Stratified Charge Engine".
4. Bullock K J, Corkill W J and Wigley G "Flow and Combustion Measurements within a Dual Chamber Stratified Charge Engine", Paper to be presented at I Mech E Stratified Charge Automotive Engine Conference, London, November 1980.
5. Launder B E and Spalding D B "Mathematical Models of Turbulence", Academic Press 1972.
6. Patankar S V and Spalding D B "A Calculation Procedure for Heat, Mass and Momentum Transfer in Three-Dimensional Parabolic Flows". Int J Heat and Mass Transfer 15 (8), 1787-1806.
7. Awn A E G "Calculation of Unsteady Compressible Flows", CHAM report 1391/2 (1977).
8. Spalding D B "Mathematical Modelling of Fluid Mechanics, Heat Transfer, and Mass Transfer Processes, a Lecture Course". Imperial College London, Heat Transfer Section: Report No. HTS/80/1 (1980).
9. Abel-Gayed R G, Bradley D and McMahon M, "Turbulent Flame Propagation in Premixed Gases: Theory and Experiment". University of Leeds, Mechanical Engineering Department (1978).
10. Gordon S and McBride B "Computer program for Calculation of Complex Chemical Equilibrium Compositions", NASA SP-273 (1971).

$\phi$	Diffusion Coefficient, $\Gamma_\phi$	Source Term, $S_\phi$
$u$	$\mu_{eff}$	$-\frac{\partial p}{\partial x}$
$v$	$\mu_{eff}$	$-\frac{\partial p}{\partial y}$
$\tilde{h}$	$\frac{\mu}{\sigma_h} + \frac{\mu_t}{\sigma_{t,h}}$	$\frac{\partial p}{\partial t}$
$k$	$\frac{\mu}{\sigma_k} + \frac{\mu_t}{\sigma_{t,k}}$	$\mu_t - \rho \epsilon$
$\epsilon$	$\frac{\mu}{\sigma_\epsilon} + \frac{\mu_t}{\sigma_{t,\epsilon}}$	$(C_1 G_k - C_2 \rho \epsilon) \frac{\epsilon}{k}$
$f$	$\frac{\mu}{\sigma_f} + \frac{\mu_t}{\sigma_{t,f}}$	0
$m_j$	$\frac{\mu_j}{\sigma_{m_j}} + \frac{\mu_{t,j}}{\sigma_{t,m_j}}$	$-R_j$

Table 1 Diffusion coefficients and source items

$\sigma_h$	0.7
$\sigma_k$	1.0
$\sigma_\epsilon$	1.0
$\sigma_f$	0.7
$\sigma_{m_{fu}}$	0.7
$C_1$	1.43
$C_2$	1.92

$\sigma_{t,h}$	0.86
$\sigma_{t,k}$	1.0
$\sigma_{t,\epsilon}$	1.3
$\sigma_{t,f}$	0.86
$\sigma_{t,m_{fu}}$	0.86
$C_D$	0.09

Table 2 Constants for the turbulence model

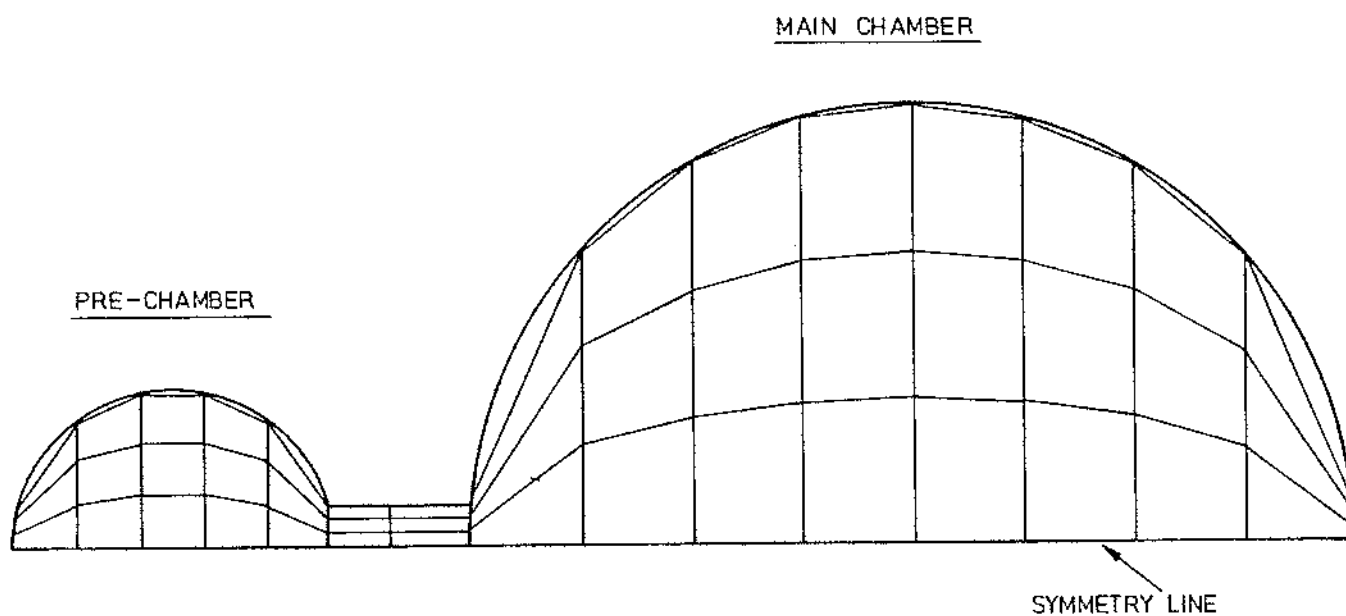


Fig. 1 Geometry of stratified charge engine and type of grid used

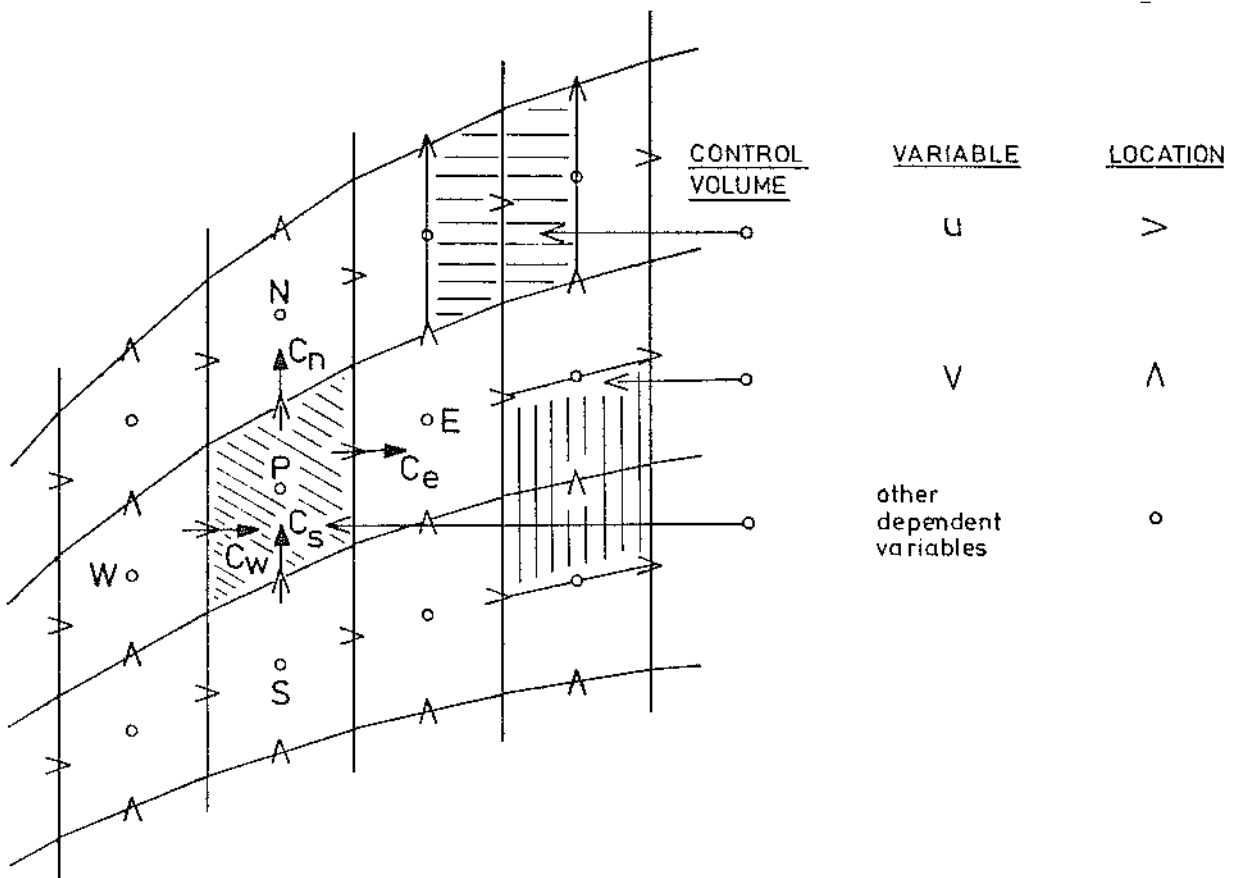


Fig. 2 Storage locations and control volumes

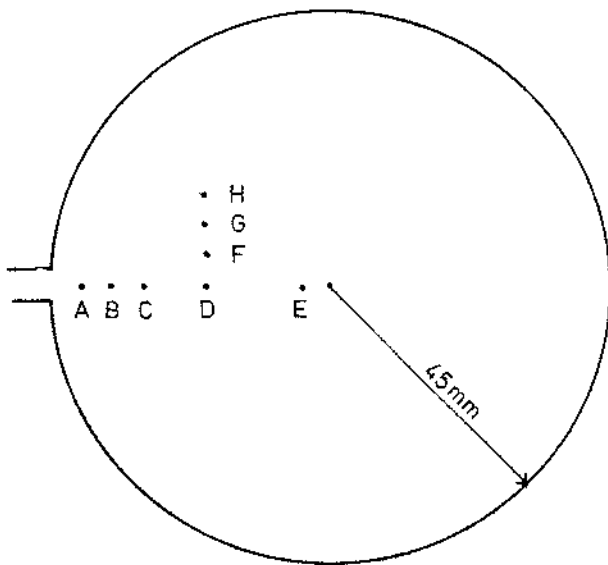


Fig. 3 Location of measurement and prediction points in main chamber for the axial  $u$  and lateral  $v$  velocity components

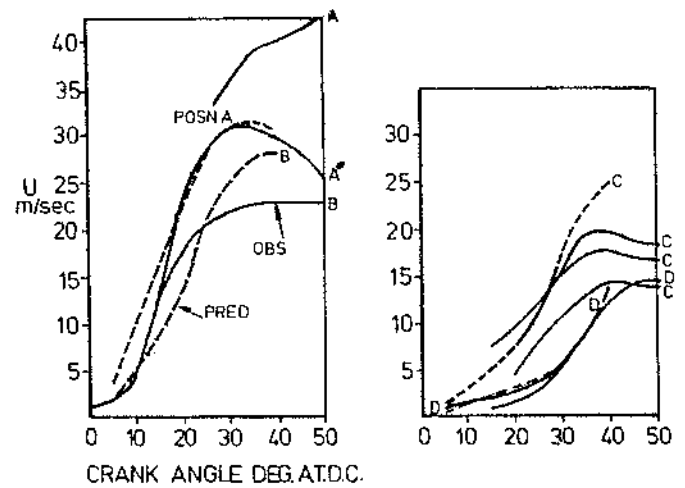


Fig. 4 LDA observations and predictions of the axial velocity component  $u$  – motored case

\* HWA corrected according to free stream temperature (reference 4)

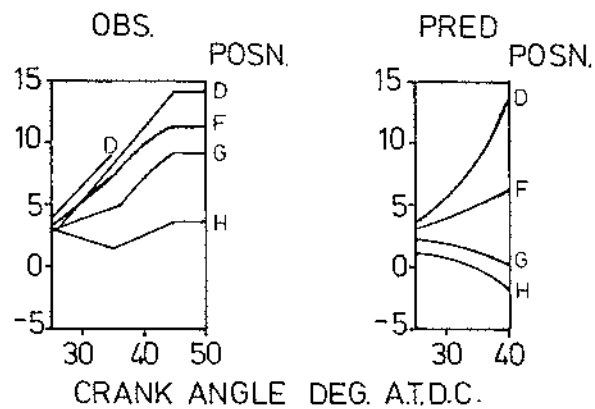


Fig. 5 LDA observations and predictions of the axial velocity component  $u$ - motored case

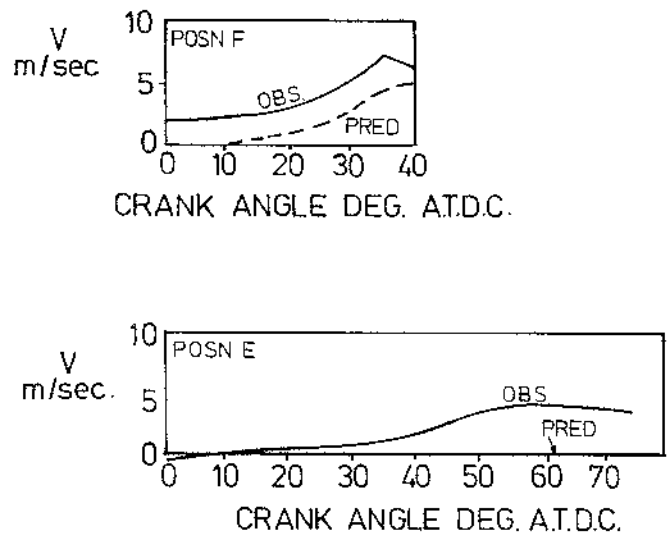


Fig. 6 LDA observations and predictions of the lateral velocity component  $v$  motored case

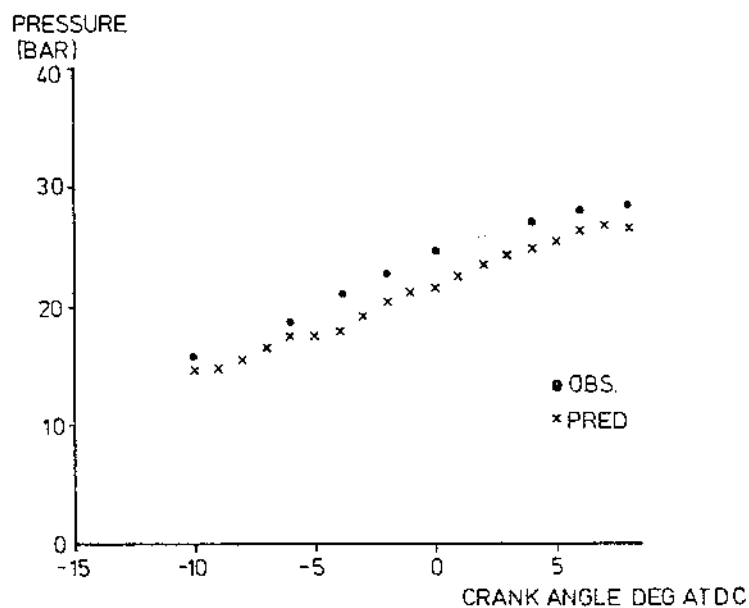


Fig. 7 Pressure vs crank angle : combustion case

